

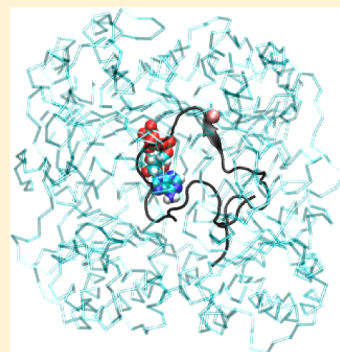
Molecular Dynamics Simulations Reveal a Novel Mechanism for ATP Inhibition of Insulin Degrading Enzyme

Carlos H. B. da Cruz and Gustavo Seabra*

Departamento de Química Fundamental, Universidade Federal de Pernambuco, Av. Jornalista Aníbal Fernandes, s/n, Cidade Universitária, Recife-PE Brazil, 50.740-560

 Supporting Information

ABSTRACT: Regulation of brain levels of the Amyloid- β 42 ($A\beta$ 42) polypeptide by IDE has recently been linked with possible routes for new therapies against Alzheimer's disease (AD). One important aspect is the regulatory mechanism of IDE by ATP, which is an IDE activator in degrading small peptides and an inhibitor in degrading larger peptides, such as $A\beta$ 42. This relationship was investigated in this study. We present molecular dynamics simulations of $A\beta$ 42 complexed with IDE, in the absence or presence of either ATP or excess Na^+ and Cl^- ions. Results suggest a previously unreported inhibition mechanism that depends on charge-induced structural modifications in the active site and interactions simultaneously involving ATP, $A\beta$ 42, and IDE. Such interactions exist only when both ATP and $A\beta$ 42 are simultaneously present in the catalytic chamber. This mechanism results in allosteric, noncompetitive inhibition with apparent decrease of substrate affinity, in accordance with experiment.



INTRODUCTION

Alzheimer's disease (AD) is the most common and devastating type of dementia, usually manifesting itself in people over 65 years old.^{1–3} The onset is marked by memory loss, followed by cognitive and motor functions decline.¹ Although the pathology is still unknown, there are strong indications relating an unusual increase in brain levels of the Amyloid- β 42 ($A\beta$ 42) polypeptide in brain regions to AD symptoms.^{4,5} This proposition was reinforced at the end of the last century through independent studies with mice genetically modified to increase the gene expression of amyloid precursor protein (APP).⁶ The rats subjected to such mutations developed some degree of dementia, which would be associated with the abnormal accumulation of amyloid- β in the brain. Impressively, the cognitive ability of these mice was restored after reduction of brain amyloid levels by enhanced activity of *Insulin degrading Enzyme* (IDE).⁷ Currently there is no cure for AD, and the treatment is only symptomatic. However, the ability of IDE to degrade $A\beta$ 42 has been considered as an alternative to the development of drugs against AD.^{8–13}

IDE is a promiscuous zinc metalloproteinase from the M16 family found in bacteria, fungi, plants, and animals.¹⁴ It was historically associated with the breakdown of insulin and, later, with the degradation of other active biomolecules including $A\beta$ 42.^{10,15} The three-dimensional structure is composed of 970 residues, distributed in four homologue domains with 25% similarity in the form of $\alpha\beta$ sandwich (Figure 1) (domain 1: residues 43–285; domain 2: residues 286–515; domain 3: residues 542–68; and domain 4: residues 769–1,011). Domains 1 and 2 form the C-terminus half (IDE-C), which is connected to domains 3 and 4 of the N-terminal half (IDE-N) by a 28 residues loop. The flexibility of this loop articulates

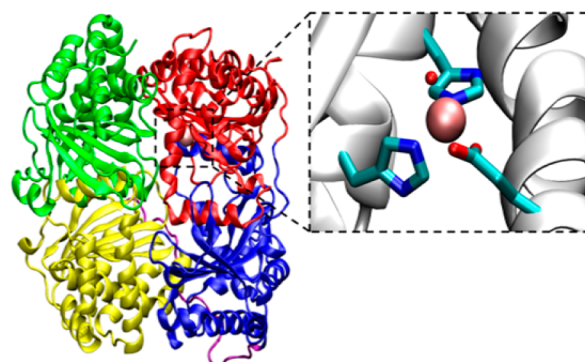


Figure 1. Crystal structure of inhibitor-free IDE (PDB: 2JG4), with the active site structure in the side. Domains 1–4 are colored red, blue, yellow, and green, respectively, and the loop connecting IDE-N and IDE-C in purple. The inset shows the structure around the active site.

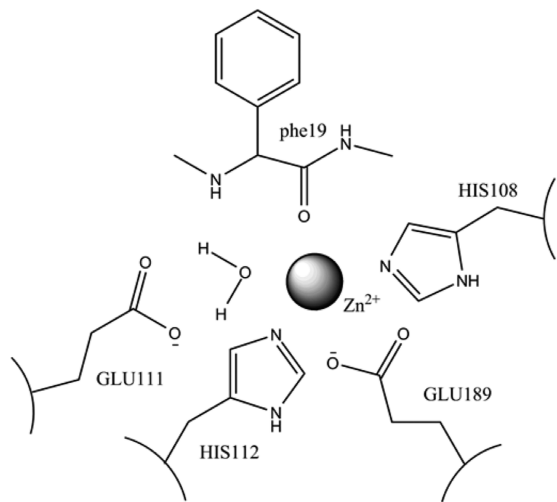
movements between the two forms of IDE: open (IDEo) and closed (IDEc) conformations.^{16,17} In the closed conformation IDE forms a catalytic chamber which size and volume can accommodate large substrates. Located on the inner wall of domain 1 within the chamber, the catalytic active site is composed of a glutamic acid (GLU111) plus an amino acid triad (HIS108, HIS112, and GLU189) with side chains linked to a Zn^{2+} ion, which sequence (HXEH) is the inverse of what is found in other enzymes of the same family (HEXXH) (Figure 1 and Scheme 1).^{10,16} In addition there is another noncatalytic site located in domain 2,30 Å away from the active site, called the distal site (formed by GLY339, GLU341,

Received: November 25, 2013

Published: April 3, 2014



Scheme 1. IDE Active Site, Shown Here in the Presence of the $\text{A}\beta$ Substrate



LEU359, VAL360 and GLY361). Its function is to facilitate and guide substrate binding with the enzyme and to increase IDE's catalytic activity through allosteric effects.^{18,19}

IDE exists as an equilibrium mixture of monomers, dimers, and tetramers, the dimers being the predominant and more active form.²⁰ The catalytic cycle starts with the substrate entry into the catalytic chamber, which can only happen when the enzyme is open (IDEo).^{14,21} The enzyme then closes, and recognition and substrate degradation processes follow. Finally, IDE opens up again for release of the degradation product and admittance of another substrate molecule (Figure 2). Studies

related to substrate size, has been the subject of some investigations.^{25–27} It has been determined that ATP and other nucleotides shift the quaternary structure of IDE from dimers to monomers²⁰ and increase the degradation rate of small substrates through a mechanism that promotes the active (open) form of IDE.²⁸ Moreover, the mechanism of inhibition has not been completely clarified yet, but the kinetic studies point to an allosteric and noncompetitive inhibition mechanism that is dependent on specific interactions between IDE-ATP and occurs with the decrease in the affinity of the substrate to the enzyme.^{23,24} To our knowledge, there is no crystallographic structure that supports these findings. Understanding the regulatory mechanism of the IDE by ATP is a challenge and has motivated research in the area, since it can open new paths for the development of alternative therapies to AD.

In this paper we show results of molecular dynamics simulations performed in an attempt to clarify the mechanism of allosteric inhibition of IDE by ATP in the cleavage of $\text{A}\beta42$ peptide. We simulated IDE complexed with $\text{A}\beta42$ in the presence and absence of ATP. To discriminate structural from charge effects, we also simulated the IDE- $\text{A}\beta42$ system in saline solution (with excess ions Na^+ and Cl^-), totaling over 380 ns of simulation time. Besides, the simulations suggest a previously unreported inhibition mechanism, in which a long substrate such as $\text{A}\beta42$ interacts with ATP in such a way as to keep IDE in the closed conformation, explaining the inhibition of the enzyme activity whenever ATP and $\text{A}\beta42$ are mutually present. This novel mechanism results in allosteric, noncompetitive inhibition and leads to an apparent decrease in substrate affinity, which is in accordance to the experimental data.²³

METHODS

Model Preparation: IDE- $\text{A}\beta42$ System. Three systems were modeled: IDE- $\text{A}\beta42$ (with no ions) and IDE- $\text{A}\beta42$ in the presence of ATP (IDE- $\text{A}\beta42+\text{ATP}$) and in the presence of NaCl (IDE- $\text{A}\beta42+\text{NaCl}$). The three molecular models were created starting from the crystallographic structure of IDE complexed with $\text{A}\beta42$ available in the PDB data bank (PDB code: 2WK3).²⁹ In this structure, all of the cysteines and the GLU111 residues were mutated during the purification and crystallization process to transform the enzyme in an inactive form. As a result a water molecule important for the catalytic mechanism, which should bind to GLU111, is also absent in the crystal structure. Due to the high mobility of $\text{A}\beta42$ within the catalytic chamber, only two small fragments were detected in the X-ray diffraction, 1–3 and 16–22. The same problem hinders the detection of a flexible loop between IDE residues SER965 and ASN979. Therefore, it was necessary to (i) restore the cysteines and GLU111 residue; (ii) reconstruct the $\text{A}\beta42$ and the missing IDE loop; (iii) introduce the water molecule near GLU111 and; (iv) fit and align the amyloid within the catalytic chamber with the crystallographic fragments fixed in the experimental position. The steps (i) and (ii) were carried out using the program DeepView (SwissPDB);³⁰ (iii) was accomplished with the program LeAP, part of the AmberTools12 distribution;³¹ and the last step (iv) with AutoDock 4.2.³² The protonation states of the titrable residues were determined with MolProbity,³³ and the SHAKE algorithm was used in all simulations.

Model Preparation: IDE- $\text{A}\beta42+\text{ATP}$ System. Starting from the previous model (IDE- $\text{A}\beta42$), ATP was docked in the IDE cationic site between ARG429, LYS898, LYS899, and SER901 residues²⁸ (Figure 3), using AutoDock 4.2.³²

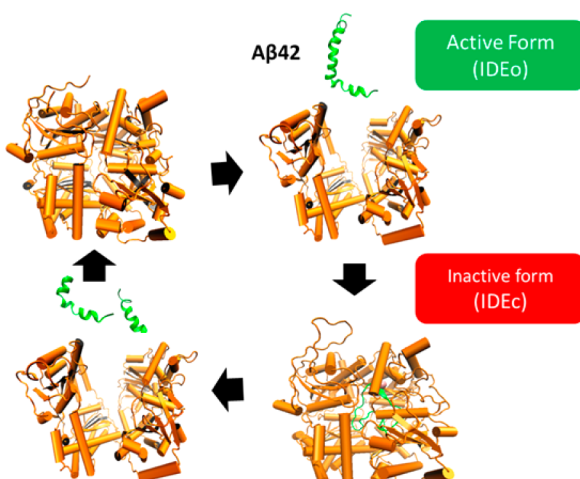


Figure 2. Illustrative scheme of the catalytic cycle of IDE (yellow) during $\text{A}\beta42$ (green) degradation.

show that IDE's catalytic activity increases with the increase of hydrodynamic radius of the enzyme⁹ and decreases with favoring the closed conformation.²² Therefore, IDEo is known as the active form and IDEc the inactive form.

Adenosine triphosphate (ATP) participates in numerous biochemical processes important for maintenance of life. In the context of this work, ATP is involved in IDE's regulation mechanism: an activator of IDE in the cleavage of small synthetic peptides, ATP is an allosteric inhibitor in the cleavage of large peptides.^{20,23,24} This ambiguity, which seems to be

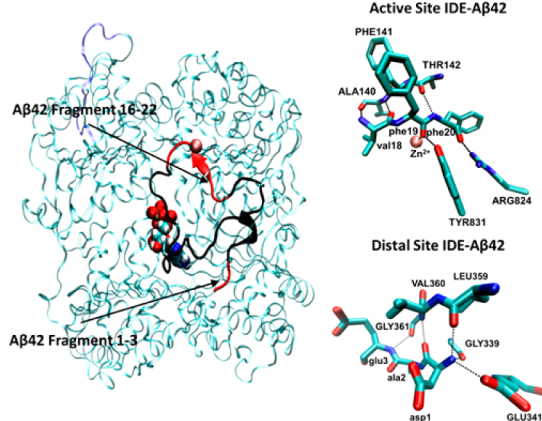


Figure 3. IDE initial structure for the simulation, after treating the PDB file as described in the text, with bound A β 42. The A β 42 fragments in black were not visible in the X-ray and were rebuilt keeping crystallographic fragments 1–3 and 16–22 (red) in the experimental positions. The rebuilt fragment 966–978 is shown in blue. ATP is shown in van der Waals spheres.

Model Preparation: IDE-A β 42+NaCl System. Starting from the IDE-A β 42 system, five extra units of Na $^+$ and Cl $^-$ were randomly placed using a Coulombic potential on a grid with 1 Å resolution around the IDE molecule. This process was carried out using the Leap program, part of the package AMBER12.³¹

Solvating. All systems were then solvated using an octahedral box with TIP3P water molecules,³⁴ keeping the distance between the enzyme and the edge of the box to a minimum of 10 Å, resulting in 20,161 water molecules added to the system without ions, 20,303 for the IDE-A β 42+ATP system and system 20,325 for the IDE-A β 42+NaCl. The complete systems were composed, respectively, of 76,884, 77,357 and 77,386 atoms.

Minimization and Molecular Dynamics Simulations. All systems were submitted to a common procedure, as described below.

Initially possible structural clashes between added water molecules and the enzyme were removed through an energy minimization with 1,000 steps of steepest descent algorithm, followed by 9,000 steps using a conjugate gradient algorithm. In both cases, only the water molecules were allowed to move. Next, the structure of the entire system was optimized with the same procedure, now with only fragments 1–3 and 16–22 of A β 42 restricted to the experimental position. Then, the systems were slowly heated from 0 to 300 K over 800 ps followed by 2 ns at the final temperature, with a temporal step equal to 1.0 fs, at constant volume.

Finally, all systems were simulated for over 40 ns with 2.0 fs time step, at 1.0 atm pressure and 300 K without any structural constraint. In all cases, the temperature was controlled using the Langevin thermostat³⁵ with a collision frequency of 2 ps⁻¹, and the pressure was controlled using the Berendsen barostat³⁶ with a pressure relaxation time of 2 ps. In all calculations, Zn in the active site was treated with the 2+ formal charge, as used in previous studies.³⁷ The AMBER ff99SB force field was used for the protein and peptide.³¹ Parameters for ATP were obtained from Meagher et al.³⁸ and, for the ions Na $^+$ and Cl $^-$, from Åqvist.^{39,40}

All energy minimization and molecular dynamics calculations were conducted with *sander* and *pmemd*, and the results were treated with the *ptraj* program, all part of the molecular

dynamics simulation package AMBER12.³¹ The secondary structure maps in Figure 7 were generated using the STRIDE method,⁴¹ available in the Visual Molecular Dynamics program (VMD).⁴²

ATP-A β 42 Binding Energy. The energy for the interaction between A β and ATP was estimated using the umbrella sampling method.^{43,44} ATP was gradually separated from the amyloid through successive molecular dynamics calculations where a harmonic potential (bias) of 60 kcal/(mol Å²) was used to restrain the distance between the center of mass (COM) of the ATP atoms and the COM of the α -carbons from ser26 and lys28. Twenty windows separated by 0.3 Å were necessary to cover the whole reaction coordinate. Initially, the initial structures in each window were generated by successive restricted geometry optimization starting from the optimized geometry from the previous window. In each optimization, 1,000 steps of with steepest descent algorithm followed by 9,000 steps with the conjugate gradient algorithm were used. Then, each umbrella window was submitted to 1.8 ns of simulation with pressure and temperature of 1.0 atm and 300 K. Finally, the results were converted into potential medium force (pmf) using the Weighted Histogram Analysis Method (WHAM),⁴⁵ with convergence tolerance of 0.0001 on the (dimensionless) free energies, using only the last 1.0 ns of each trajectory.

Replicas. Replicas of all the systems were simulated to evaluate the existence of simulation artifacts. The initial structure of each replica simulation was chosen by clustering the original trajectories into three clusters with the hierarchical algorithm, using the amyloid backbone atoms' RMSD as metric (Table 2). The representative structure of the lowest occurrence cluster was used as the initial structure of the molecular dynamics, and the simulations were conducted using the same protocol of the original system. In the case of the simulation without ions, this structure had the bond between TYR831 and phe19 (d9) already broken, which lead to inconsistent results (see Discussion). Therefore, we run a third replica of this system starting from the representative structure of cluster 2.

RESULTS

In this study, IDE complexed with amyloid was simulated in aqueous solution and in three different situations: with no ions, in the presence of ATP docked to its binding site, and in the presence of excess sodium chloride, on an attempt to elucidate the mechanism by which ATP inhibits IDE in the breakdown of amyloid. For this purpose, it was necessary to determine the binding site of the ions, analyze the dynamics of IDE and amyloid in the presence and absence of ions in terms of RMSF, RMSD, and analysis of secondary structure, and estimate the binding energy of ATP-A β 42.

Equilibration. MD simulations were monitored through the Root Mean Squared Deviation (RMSD) of the backbone atoms of IDE as a function of time (Figure 4 and S1), taking as a reference the initial structure of each simulation. The RMSD values for systems without ions (No Ions), with ATP (ATP) and in saline solution (NaCl) stabilize after 10, 20, and 10 ns, respectively. All analyses shown from now on were performed disregarding the structures prior to RMSD stabilization.

Location of ATP Ions Inside the Catalytic Chamber. Figure 5A shows the number of hydrogen bonds ATP makes with either A β 42 or IDE as a function of time. Hydrogen bonds were assumed whenever the distance between the donor (D)

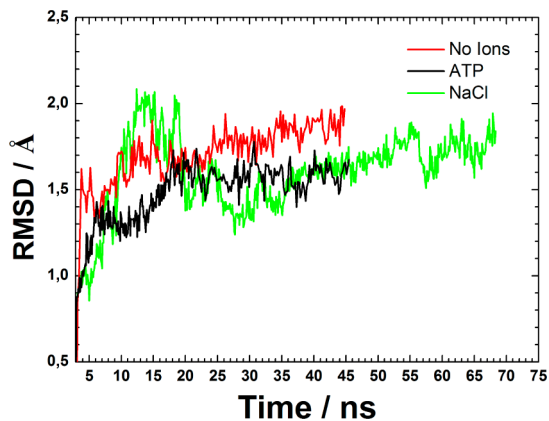


Figure 4. RMSD for IDE backbone atoms (C, N, O) as a function of time, taking as reference the first structure in each simulation.

and acceptor (A) atoms and the A–H–D angle were less than 3.0 Å and larger than 110°, respectively.⁴⁶ The simulations show that, in the IDE- $\text{A}\beta 42$ +ATP system, ATP tends to interact both with the $\text{A}\beta 42$ and IDE residues.

ATP was initially docked in the experimental position between ARG429, LYS898, LYS899, and SER901 residues.²⁸ However, in the course of the simulation, ATP migrates to a neighboring region rich with polar amino acids, losing the LYS898, LYS899, and SER901 interactions and establishing new interactions with the enzyme and the substrate (see Video S1). The nucleotide maintains a strong interaction with the ARG429 and forms new hydrogen bonds with LYS85, ARG431, and ARG892 of the IDE via the triphosphate motif and, at the same time, with the ser26 and lys28 of the amyloid (Figure 5B), as shown in Table 1, effectively creating a bridge connecting the two halves of the enzyme. This migration is not surprising, since experimental position was determined in the absence of the substrate, which offers new possibilities for interaction. The same behavior was observed in the replica (see Figure S2).

The fact that ATP interacts with the enzyme and amyloid through the triphosphate motif suggests that other nucleotides can produce the same effect. In fact, there are reports in the literature that the mechanism of IDE inhibition may depend

Table 1. Occupation of Hydrogen Bonds Formed by ATP^c

residue ^a	occupation ^b
ARG429	98 (96)
LYS85	35 (13)
ARG431	83 (99)
ARG892	45 (23)
ser26	26 (23)
lys28	28 (99)

^aIDE residues are indicated with uppercase 3-letter code, and amyloid residues are indicated with lowercase codes. ^bOccupation measured as percentage of total simulation time. ^cThe values in parentheses indicate the occupation for the replica.

not only on ATP but also on other nucleotides, such as GTP, ADP, and PPPi,²³ in agreement with the inhibition mechanism proposed.

Location of Chlorides Ions inside the Catalytic Chamber. Not only ATP but also other ions have the ability to connect to IDE and activate the enzyme via allosteric effects. High concentrations of NaCl have also been found to produce similar effects.²⁸ Thus, we also evaluated the behavior of IDE complexed with amyloid in the presence of five extra units of Na^+ and Cl^- .

The simulations indicate that the chloride ions show a clear preference for some specific regions of the catalytic chamber. The regions preferentially occupied by the Cl^- were determined by the percentage of the total frames in which a Cl^- ion is found within 4.0 Å from an ALA or LYS residue. The sites with the largest occupation are shown in Figure 6. It is possible to distinguish three main binding sites (S1, S2, and S3) near which the chloride ions appear during 41, 36, and 13% of the simulation time in the original system and 50, 84, and 26% in the replica, respectively. The occurrence of the binding sites S1, S2, and S3 in the replica reinforces the results presented here. S1 site lies on the IDE-C and is composed of the amino acids ARG429, ARG892, LYS898, and LYS899. It has been experimentally related to the allosteric activation of IDE by anions.²⁸ The second site is located in IDE-N, about 10 Å away from the active site, and is formed by one amino acid from IDE (LYS192) and another from the amyloid (lys16). It is possible that the short distance between the chloride ion connected on

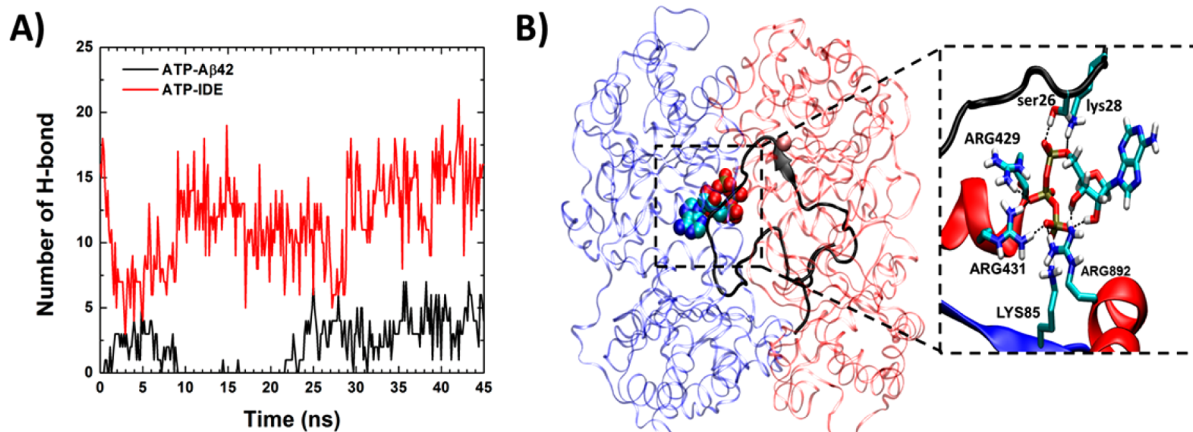


Figure 5. A) Number of hydrogen bonds between ATP and $\text{A}\beta 42$ (black line) and ATP and IDE (red line), as a function of time. B) IDE- $\text{A}\beta 42$ +ATP complex. Left: The enzyme structure is represented in ribbons, while spheres represent ATP (light blue: carbon, blue: nitrogen, red: oxygen and white: hydrogen) and Zn (salmon). ATP binds to the internal wall between IDE-C (red) and IDE-N (blue). Right: Enlarged view of the ATP binding site, showing the main ATP-IDE and ATP- $\text{A}\beta 42$ interactions.

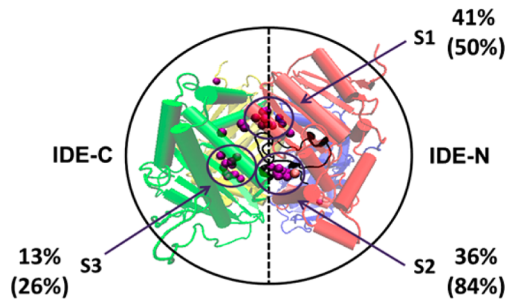


Figure 6. (A) Occurrence of Cl⁻ ions within 4.0 Å of ALA and LYS side chains. (B) Top views of the main Cl⁻ ions binding sites in IDE (S1, S2 and S3). Site occupancy, calculated in terms of occurrence of Cl⁻ ions within 4.0 Å of ALA and LYS side chains, is shown to the original system and in parentheses for the replica.

S2 and the metal center cause an imbalance in the active site charges, resulting in significant changes in the reaction profile. Finally, S3 is located in IDE-C and is composed of the amino acids LYS632, ARG687, and LYS697. However, the low occurrence of chloride ions (about 13%) indicates little or no influence on the activation mechanism. No specific interactions were seen between the chloride connected to the cationic site (S1) and the A^β42 peptide.

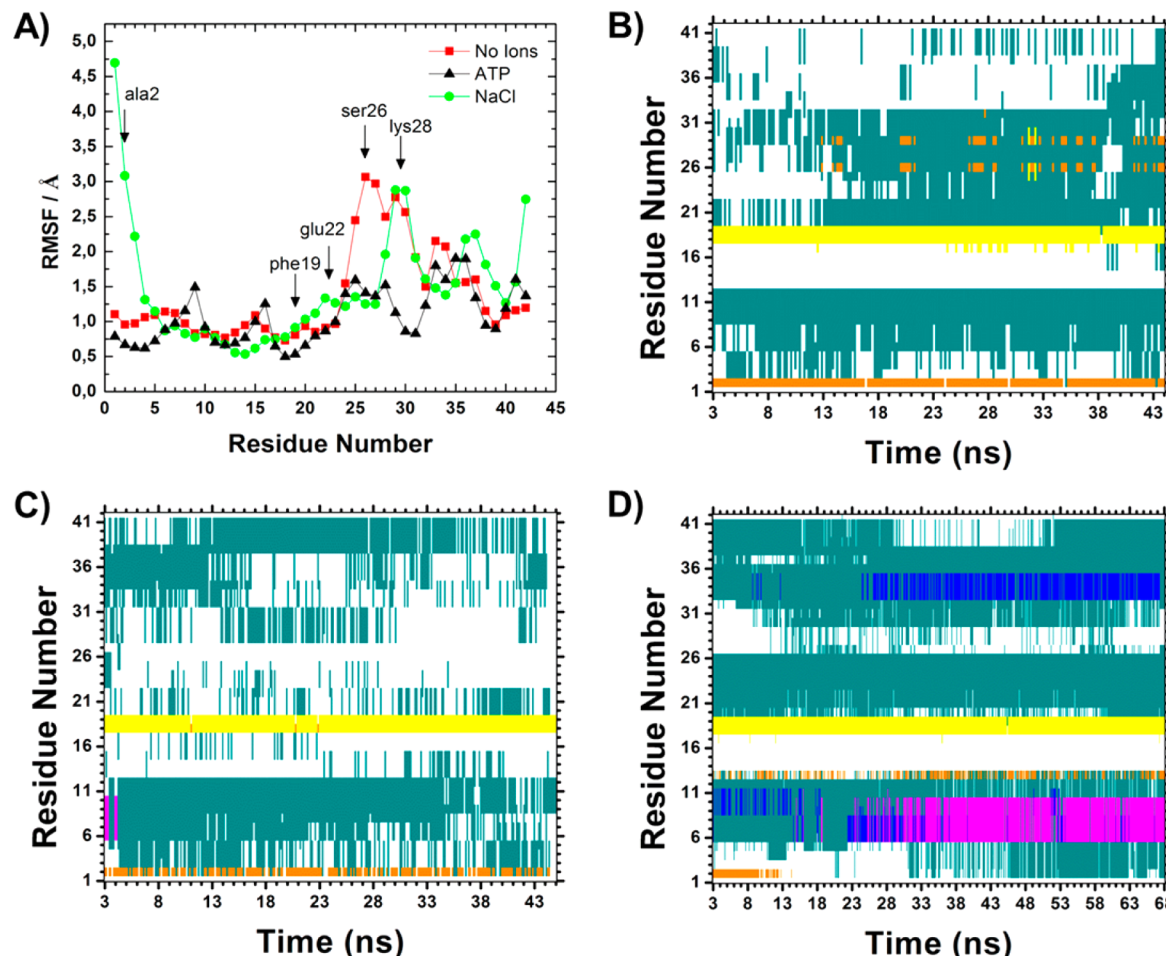


Figure 7. (A) A^β42 backbone RMSF obtained for the systems with no ions (red squares), in the presence of ATP (black triangles) and in saline solution (green circles). Residues from the substrate involved in the bonding to IDE are indicated (B–D) Secondary structure of IDE+A^β42 in the system with no ions (B), in the presence of ATP (C) and NaCl (D). Green: turn; Yellow: β-sheet; Orange: isolated bridge; Pink: α-helix; Blue: 3–20 helix; and White: random coil.

Structural Analysis of the Amyloid inside the IDE-A^β42 System in the Presence and Absence of Ions. The effect of ions in the activation of IDE has been documented in the literature,²⁸ but the influence of ions in the inhibition mechanism of IDE is still not very clear.

The simulation results presented here suggest some previously unreported molecule interactions that may prove critical to the mechanism of IDE regulation by ATP. The impact of ATP and Cl⁻ ions in the A^β42 structure were analyzed in terms of Root Mean Square Fluctuation (RMSF) and secondary structure map. In Figure 7A the backbone RMSF for the A^β42 in the three systems is compared, along with the secondary structure map for each system in Figure 7 B, C, and D. The secondary structure maps of amyloid in the absence (Figure 7B) and presence of ATP (Figure 7C) show the formation of bridges to ala2 amino acid and β-sheet on fragment 18–19 with low RMSF value (low Flexibility) (Figure 7A). In the absence of ATP, unstable isolated bridges are formed between the amino acids ser26 and lys28 after 12 ns. These interactions are weak and incapable of significantly reducing this region's flexibility. On the other hand, in the presence of ATP, the low values of RMSF fragment 22–33 can be attributed to the interactions between the ATP and ser26 and lys28 amino acids.

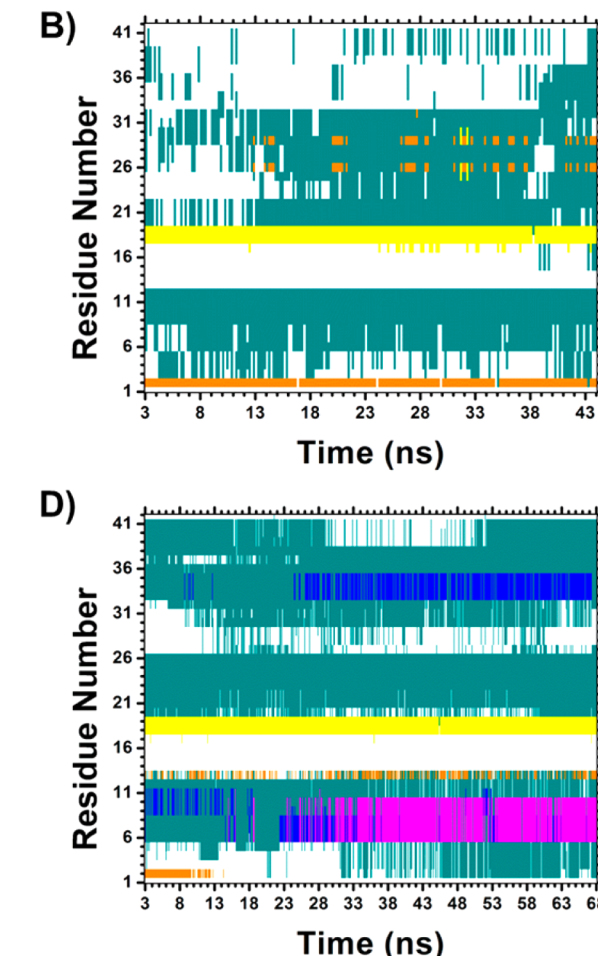


Figure 7. (A) A^β42 backbone RMSF obtained for the systems with no ions (red squares), in the presence of ATP (black triangles) and in saline solution (green circles). Residues from the substrate involved in the bonding to IDE are indicated (B–D) Secondary structure of IDE+A^β42 in the system with no ions (B), in the presence of ATP (C) and NaCl (D). Green: turn; Yellow: β-sheet; Orange: isolated bridge; Pink: α-helix; Blue: 3–20 helix; and White: random coil.

The presence of bound chloride ions in the IDE-C changes the electrostatic environment so that the β -sheet 1–3 is dismantled in the presence of chloride ions (Figure 7D). This occurs with significant increase of the RMSF on this region (Figure 7A), indicating the detachment of fragment 1–3 from the distal site. In addition to these, other structures are visible during most of the time. For example, the presence of chloride ions induces the formation of α and 3–20 helices in the 5–9 and 33–35 fragments, respectively. The first occurs shortly after the unraveling of β -sheet 1–3 (13 ns), and the second after 25 ns of simulation. Both are stable structures and occur with a reduction on the flexibility of fragments 5–9 and 33–35 of amyloid. Finally, we note the intermittent formation of bridges to his13 along the trajectory.

Structural Analysis of IDE in the Presence and Absence of Ions. The presence of ions results in changes sometimes significant, in the dynamics of IDE, which could be related to the open-and-closing motion of the enzyme. Figure 8

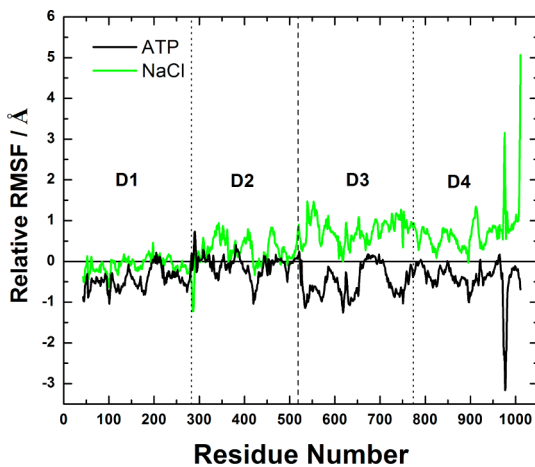


Figure 8. RMSF of IDE backbone atoms (C, N and O) of the system with ATP (black) and saline solution (green), relative to the system without ions.

shows the relative RMSF for IDE backbone atoms of the system with ATP (black) and saline solution (green), taking as reference the IDE on system IDE-A β 42 (no ions), offering an overview of the flexibility (RMSF) relative of the IDE-N and IDE-C after the addition of ions.

The IDE-N relative RMSF (domain 1 and 2) in the presence of ions is close to zero, indicating that this portion of IDE does not suffer direct influence of the environment. In fact, the ions are bound in a common site located in IDE-C and not in IDE-N. In contrast, the flexibility of IDE-C is reduced in the presence of ATP and increased in NaCl solution, suggesting that the ATP-A β 42 interaction is holding the enzyme in the closed conformation and is stronger than the anion activator effect.

ATP-A β 42 Binding Energy. In our approach, the bound ATP in the cationic site interacts with the amyloid which is connected on the other half of the IDE, creating a connection between the halves of IDE reducing the enzyme movements. These results indicate that ATP-A β 42 interactions are responsible for holding the IDE in its closed (inactive) form. As another test to this assumption, we calculate the energy of the ATP-A β 42 interaction. The energy of this interaction is the necessary increment needed to open the enzyme, as compared

to the energy for opening the IDE when complexed with the amyloid alone.

Figure 9 shows the variation of the pmf as a function of distance between the ATP and the amyloid fragment 26–28. A

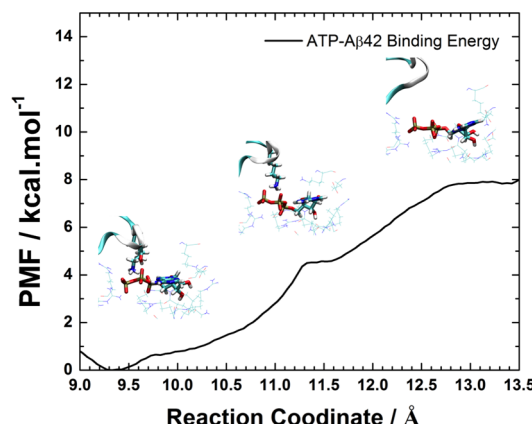


Figure 9. Potential of Mean Force (PMF) profile of the process of breaking the ATP-A β 42 interactions. The pictures within the graphic show the loss of interaction ATP-A β 42 along the reaction coordinate.

minimum of energy is located when the distance between the two groups' COMs is 9.3 Å, indicating that the ATP-A β 42 interaction is more effective at this distance. As the distance is increased the ATP-ser26 interaction is broken first, and the ATP-lys28 interaction breaks when the distance is 11.3 Å and requires about 4.5 kcal/mol to be broken. The last interaction with the substrate is disrupted when the distance between the ATP and fragment 26–28 is equal to 12.8 Å. The whole process requires about 7.8 kcal/mol.

Amyloid Recognition by IDE in the IDE+A β 42 System and Ion Effects. A β 42 connects to IDE via two small fragments, 1–3 and 16–22. The first fragment interacts in the distal site forming a small β -sheet with IDE-N fragment 341–363. At the same time, the second fragment interacts with the active site residues to form another discrete β -sheet with the IDE-N residues 140–145.²² All these interactions are part of the enzyme–substrate recognition mechanism and were reproduced recently by molecular dynamics simulations from another group.⁴⁷ Similar structures were also detected in our simulations.

We observe that the N-terminal tail of the amyloid interacts with the distal site and forms an isolated bridge between the VAL360 and ala2, which is stabilized by the d1-d4 hydrogen bonds (HB) (Figure 10A). Interactions d1, d2, and d3 are formed between the asp1 nitrogen and GLY339, LEU359, and GLU341 residues, whereas d4 is formed between the backbone oxygen of GLY361 and asp1 nitrogen. Meanwhile, the val18 and phe20 residues of the substrate interact with the THR142 (d5 and d6) and ALA140 (d7) residues to form a small β -sheet, which is stabilized by hydrogen bonds formed between the amine groups of ARG824 and the oxygen of phe20 (d8) and between the hydroxyl oxygen of TYR831 and the carbonyl oxygen of phe19 (d9). Additionally, the zinc ion interacts strongly with the amyloid peptide and forms with HIS108, HIS112, and GLU189 a metal–ligand coordination complex (Figure 10B). This last structure is maintained throughout the simulation, with the distance between the zinc ion and phe19 oxygen around 2.9 (± 0.7), 3.0 (± 0.7), and

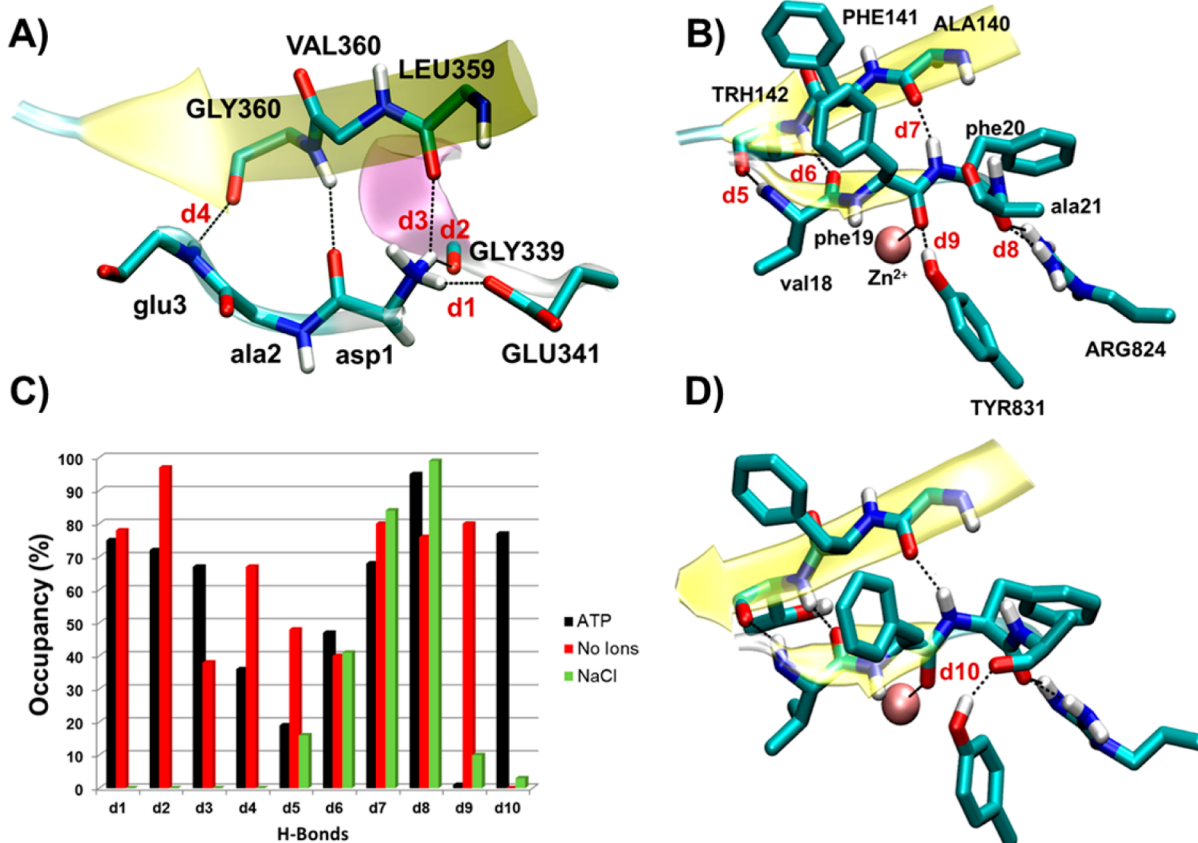


Figure 10. Representative structure of Ab42 fragments 1–3 and 18–21 bound to IDE. (A) The main interactions between $\text{A}\beta$ 42 fragment 1–3 and the IDE distal site (d1-d4); (B) Interactions between $\text{A}\beta$ 42 fragment 18–21 and IDE active site (d5-d10); (C) Occupancy of hydrogen bonds between $\text{A}\beta$ 42 fragment 1–3 and the IDE distal site and the $\text{A}\beta$ 42 fragment 16–22 and IDE active site; (D) The d10 hydrogen bond formed between TYR831 and ala21 residues.

2.1 (± 0.5) Å for systems no ions, with ATP and in NaCl, respectively.

The presence of ions, ATP in particular, induces specific changes in the distal and active site. The occupancy of the hydrogen bonds in the distal site (d1-d4) is affected in the presence of ATP, being 35% lower in d4 (Figure 10C, S3). Of the interactions responsible for holding the amyloid in the active site (d5-d9 and d10), one can note a marked decrease in d5 occupation and the complete disappearance of the d9 bond in the presence ATP (Figure 10C, S3). The nucleotide interacts strongly with the amyloid C-terminal tail, inducing conformational changes in the active site region. This interaction is responsible for the disappearance of d9 and formation of the HB between the hydroxyl hydrogen of TYR831 and the carbonylic oxygen of ala21 (d10) (Figure 10D). The loss of the interaction d9 reduces the interactions responsible for fixing the substrate in a suitable position for the reaction, destabilizing the intermediate proteolytic. Thus, one should expect an increase in the energy barrier and consequently reducing the enzymatic kinetics. This hypothesis is currently being investigated via hybrid calculations of type QM/MM in the presence and absence of ATP and will be shown in a subsequent publication.

In saline solution, interactions responsible to hold the amyloid N-terminal tail to the distal site (d1-d4) are broken, resulting in the dismantling of the 1–3 β -sheet and detachment of the amyloid N-terminal tail from distal site, as shown by the RMSF data in Figure 7A. We also note that geometrical changes around the active site are very similar to those

observed in the ATP system, indicating that the charge contributes through nonspecific effects to the geometric changes in the active site.

Replicas. The equilibrated trajectory of each system was grouped in three clusters, as listed in Table 2 from lowest to

Table 2. Percent Population of the Clusters Sampled by the Original Simulations

cluster	No Ions	ATP	NaCl
1	24.3	3.6	19.4
2	35.2	21.8	21.5
3	40.5	74.6	59.1

highest occurrence. Initially the replicas were simulated using the representative structure of the lowest occurrence cluster. However, the replica system without ions showed results inconsistent with the crystallographic data. For example, the TYR831-phe19 bond (d9), which is detected in X-ray, was broken at the beginning of the calculation, and the C-terminal tail of amyloid twists and adopts a conformation that favors TYR831-glu23 bond. Therefore, a new replica was simulated using the representative structure of cluster-2 as the initial structure of the simulation. This may show a similar behavior as the original system, indicating that the conformation of amyloid in the enzyme determines the pattern of IDE- $\text{A}\beta$ 42 binding. On the other hand, the replicas of other systems (ATP and NaCl) reproduced all results of the original simulations, indicating that the presence of ATP results in genuine phenomena that are

closely related to the ATP charge and specific interactions between IDE-ATP, ATP- $\text{A}\beta$ 42, and $\text{A}\beta$ 42-IDE.

■ DISCUSSION

IDE can be activated in two ways: homotropic or heterotropic allosteric activation.^{20,23,25,28,48} The IDE homotropic activation occurs when a long substrate interacts with the distal site of one subunit IDE, inducing conformational changes on the neighboring subunit. This activation model is strongly related to the concept of symmetric allosteric activation, in which a molecule bonded in subunit A produces allosteric effects that culminate in the activation of subunit B. Heterotropic activation by small peptide or ATP occurs through two distinct mechanisms. The first is associated symmetric allosteric activation, which happens when a small peptide mimics the effect of a large substrate. In this case, the activation is nonspecific to substrate size and is only possible on dimeric IDE. In the second case, sequential allosteric activation, the connection between the subunits is broken in the presence of ATP and the activation occurs in the subunit to which ATP is bound. Curiously, IDE activation by ATP only happens during the degradation of small substrates and not during the degradation of large substrates. Regardless of the mechanism of activation, either symmetrical or sequential, IDE activation occurs by increasing the population of open enzymes (active).^{9,22} Therefore, it is speculated that the mechanism of inhibition of IDE associated with favoring the closed conformation (inactive).

The insulin degradation inhibition by ATP *in vivo* was first reported in 1987 by Hashimoto⁴⁹ and subsequently induced by ATP plus aluminum fluoride.⁵⁰ In 2001, Camberos et al. demonstrated that ATP in the presence of Mn²⁺ (or Mg²⁺) inhibits the activity of purified IDE (*in vitro*) in the degradation of insulin.²³ It was speculated that ATP and other chemically similar molecules could bind to a common domain in IDE, thus reducing the volume available for the complexation of a substrate or inducing conformational changes in the substrate which is proteolytically inappropriate.¹³ The facts presented above summarize a decade of debates and still the mechanism of ATP inhibition of IDE is still unknown. This reflects the difficulty involved in these processes and opens the way for molecular modeling and the systematic study of protein–protein interactions.

Motivated by the latest research, we created a molecular model of IDE complexed with amyloid in the presence of ATP (Figure 3). To justify the presence of ATP within the IDE complexed with $\text{A}\beta$ 42 and explore this hypothesis, we made the following assumption: It is known that ATP binds to the cationic site localized in IDE-C,^{28,51} while substrates binds to the other half of the enzyme (IDE-N).²² So it is reasonable to assume that, being a small molecule and with fewer degrees of freedom, ATP reaches the cationic site and binds IDE more easily than the amyloid, a long substrate. It is also known that Mn²⁺ and Mg²⁺ ions are required for inhibition. These ions protect IDE from denaturation and are an accessory to ATP binding to proteins.²³ In the present work, however, since we are already considering ATP bound to the protein and the time scale of the simulations do not allow for denaturation, it is unlikely that their presence will influence the results. So, we opted to not include them in the simulations, which allows us to better isolate the ATP contribution to inhibition.

Once inside the IDE and in the absence of substrate, ATP breaks the electrostatic equilibrium that holds the enzyme in

the closed conformation, increasing the population of open enzymes.²⁸ Given the distance between the two sites, it is reasonable to assume that the amyloid can still bind to the open IDE in the presence of ATP. After the amyloid binding, IDE would close and try to initiate the normal substrate recognition and degradation mechanism. In this scenario, it is reasonable to assume that ATP and amyloid can coexist within IDE and initiate the effect that leads to inhibition of enzymatic activity. Our simulations show that the bond IDE-ATP is stable in the presence of amyloid, suggesting the Michaelis-Menten complex can still exist in this configuration.

Amyloid is an insoluble and disordered protein, with high capacity to form aggregates in the form of β -sheet.^{52–56} From the computational point of view, the molecular dynamics simulations of disordered proteins such as $\text{A}\beta$ in solution requires long simulation time for sampling the configurational space and determined events of nucleation and formation of molecular aggregates.^{53,57} In our case, however, one unit of the amyloid is captured by IDE and confined within the enzyme's catalytic chamber, with a volume of 1,300 Å³. The amyloid then interacts with the chamber through the active and distal sites, forming a structure stable enough that some residues can be detected by X-ray diffraction: Fragments 1–3 and 16–22 are anchored inside the IDE, limiting the amyloid's movement and allowing new possibilities for interaction.¹⁷ The result shows that the amyloid, which has a disordered structure in solution, adopts a somewhat restricted tridimensional arrangement within IDE. In the presence of ATP, the accessible volume of the substrate decreases, further restricting the movement of the substrate within the confined environment. Thus, molecular dynamics simulations under these conditions allow the conformational space available for the amyloid to be sampled in only a few tens of nanoseconds, as was noted in a previous study by Bora et al.⁴⁷ Similarly, the structure of our system is stabilized at about 10–20 ns.

We have chosen to place the amyloid inside the enzyme such as to reproduce these interactions, but it is evident that the conformation adopted by the peptide inside IDE cannot be limited to this one case: IDE is a versatile enzyme, capable of breaking the amyloid in a variety of peptide bonds, (val12-his13, his14-gln15, phe19-phe20, lys28-gly29, etc.) allowing a large number of binding configurations. Nevertheless, the fact that the X-ray shows the amyloid interacting with the active site through phe19-phe20 residues suggests this configuration as the most probable.

Our simulations show that ATP binds to IDE-C and interacts with the amyloid, which is connected to IDE-N, creating a bridge that connects the two halves of the IDE restricting the movements of the enzyme and substrate. Such interaction induces a conformational change in the substrate that appears to be proteolytically unfavorable for the catalytic reaction and contributes to increase the opening energy of the IDE by, at least, around 8 kcal/mol. Whereas the opening movement of the enzymes are in the order of $k_{\text{b}}T$,^{58,59} an increment of 8 kcal/mol for the opening process is sufficient to hold the enzyme in the closed conformation.

The present data is, admittedly, not sufficient to access the full large scale opening motion of IDE. This supposition would be fully refined by calculating the energy landscape for the conformational transition of opening IDE- $\text{A}\beta$ 42 in the absence and presence of ATP. We are currently investigating this transition, in order to clarify these effects, by using the nudged

elastic band method (NEB)⁶⁰ and molecular dynamics simulations using target umbrella sampling method.^{43,44}

The idea that the IDE inhibition mechanism by ATP in the cleavage of $\text{A}\beta_{42}$ can occur through an effect favoring the closed form would not be the first example of its kind. The literature has reported similar effects on proteins that have the same behavior. For example, the phosphotransferase enzyme adenylate kinase (AdK) is a multiconfiguration protein which changes the conformational landscape with the binding of inhibitor.⁵⁹ According to the authors, in the binding state, the interaction of the inhibitor with the two halves of the AdK favor the closed form, while the open form of the enzyme is more favorably in the unbound state.

Together, these effects reduce the catalytic turnover and lead to an apparent reduction of the IDE affinity, in agreement with the experimental data.²³

CONCLUSIONS

Once inside IDE, the anions bound in cationic site should, in principle, exert the same effect. However, we observed opposite effects that do not depend only on charge but also on the specific IDE-ATP, ATP- $\text{A}\beta_{42}$, and IDE- $\text{A}\beta_{42}$ interactions. These interactions favor the closed conformation of IDE and restrict the open-and-close movement of enzyme, necessary to release of the reaction products and entry of a new substrate molecule. This effect depends directly on the substrate size, since any substrate binds the catalytic half (IDE-N), but only long substrates are capable of interacting simultaneously with IDE-C intermediated by ATP. The practical result is IDE inhibition toward the degradation of the $\text{A}\beta$, when in the presence of ATP.

The possibility of inhibition occurring with the substrate inside the catalytic chamber opens new perspectives for the modeling of drugs for Alzheimer's disease that act by blocking the cationic site, thereby increasing the enzyme activity. New experimental studies should look for evidence of the simultaneous presence of $\text{A}\beta_{42}$ and ATP within the IDE.

ASSOCIATED CONTENT

Supporting Information

Figures S1, S2, and S3 as well as video S1. This material is available free of charge via the Internet at <http://pubs.acs.org>.

AUTHOR INFORMATION

Corresponding Author

*E-mail: gustavo.seabra@gmail.com.

Author Contributions

The manuscript was written through contributions of all authors. All authors have given approval to the final version of the manuscript. All authors contributed equally.

Notes

The authors declare no competing financial interest.

ACKNOWLEDGMENTS

This work was made possible by financial support from Fundação para o Amparo à Ciência e Tecnologia do Estado de Pernambuco (FACEPE), grant APQ-1473-1.06/10, and Instituto Nacional de Nanotecnologia para Marcadores Integrados (INAMI). Computer time was provided by the Centro Nacional de Processamento de Alto Desempenho em Pernambuco (CENAPAD-PE) and Oak Ridge Leadership Computing Facility.

REFERENCES

- (1) Alzheimer's Association. *Basics of Alzheimer's Disease*; London, 2005; p 17.
- (2) Alzheimer's Association. *2009: The Year in Alzheimer Science*; London, 2009; p 623.
- (3) Alzheimer's Association. *Alzheimer's Disease Facts And Figures*; London, 2012; Vol. 8, p 72.
- (4) Qiu, W. Q.; Folstein, M. F. Insulin, Insulin-Degrading Enzyme and Amyloid-Beta Peptide in Alzheimer's Disease: Review and Hypothesis. *Neurobiol. Aging* **2006**, *27*, 190–198.
- (5) Bernstein, H.-G.; Ansorge, S.; Riederer, P.; Reiser, M.; Frölich, L.; Bogerts, B. Insulin-Degrading Enzyme in the Alzheimer's Disease Brain: Prominent Localization in Neurons and Senile Plaques. *Neurosci. Lett.* **1999**, *263*, 161–164.
- (6) Lewis, J.; Dickson, D. W.; Lin, W. L.; Chisholm, L.; Corral, A.; Jones, G.; Yen, S. H.; Sahara, N.; Skipper, L.; Yager, D.; Eckman, C.; Hardy, J.; Hutton, M.; McGowan, E. Enhanced Neurofibrillary Degeneration in Transgenic Mice Expressing Mutant Tau and APP. *Science* **2001**, *293*, 1487–1491.
- (7) Leissring, M. A.; Farris, W.; Chang, A. Y.; Walsh, D. M.; Wu, X.; Sun, X.; Frosch, M. P.; Selkoe, D. J. Enhanced Proteolysis of Beta-Amyloid in APP Transgenic Mice Prevents Plaque Formation, Secondary Pathology, and Premature Death. *Neuron* **2003**, *40*, 1087–1093.
- (8) Zhao, L.; Teter, B.; Morihara, T.; Lim, G. P.; Ambegaokar, S. S.; Ubeda, O. J.; Frautschy, S. A.; Cole, G. M. Insulin-Degrading Enzyme as a Downstream Target of Insulin Receptor Signaling Cascade: Implications for Alzheimer's Disease Intervention. *J. Neurosci.* **2004**, *24*, 11120–11126.
- (9) Im, H.; Manolopoulou, M.; Malito, E.; Shen, Y.; Zhao, J.; Neant-Fery, M.; Sun, C.-Y.; Meredith, S. C.; Sisodia, S. S.; Leissring, M. A.; Tang, W.-J. Structure of Substrate-Free Human Insulin-Degrading Enzyme (IDE) and Biophysical Analysis of ATP-Induced Conformational Switch of IDE. *J. Biol. Chem.* **2007**, *282*, 25453–25463.
- (10) Authier, F.; Posner, B.; Bergeron, J. Insulin-Degrading Enzyme. *Clin. Invest. Med.* **1996**, *19*, 149–160.
- (11) Wang, D.-S.; Dickson, D. W.; Malter, J. S. Beta-Amyloid Degradation and Alzheimer's Disease. *J. Biomed. Biotechnol.* **2006**, *2006*, 58406.
- (12) Mirsky, I. A.; Broh-Kahn, R. H. The Inactivation of Insulin by Tissue Extracts; the Distribution and Properties of Insulin Inactivating Extracts. *Arch. Biochem.* **1949**, *20*, 1–9.
- (13) Cabrol, C.; Huzarska, M. A.; Dinolfo, C.; Rodriguez, M. C.; Reinstatler, L.; Ni, J.; Yeh, L.-A.; Cuny, G. D.; Stein, R. L.; Selkoe, D. J.; Leissring, M. A. Small-Molecule Activators of Insulin-Degrading Enzyme Discovered through High-Throughput Compound Screening. *PLoS One* **2009**, *4*, e5274.
- (14) Becker, A. B.; Roth, R. A. Insulysin and Pitrilysin: Insulin-Degrading Enzymes of Mammals and Bacteria. *Methods Enzymol.* **1995**, *248*, 693–703.
- (15) Farris, W.; Mansourian, S.; Chang, Y.; Lindsley, L.; Eckman, E. A.; Frosch, M. P.; Eckman, C. B.; Tanzi, R. E.; Selkoe, D. J.; Guenette, S. Insulin-Degrading Enzyme Regulates the Levels of Insulin, Amyloid Beta-Protein, and the Beta-Amyloid Precursor Protein Intracellular Domain in Vivo. *Proc. Natl. Acad. Sci. U. S. A.* **2003**, *100*, 4162–4167.
- (16) Li, P.; Kuo, W.-L.; Yousef, M.; Rosner, M. R.; Tang, W.-J. The C-Terminal Domain of Human Insulin Degrading Enzyme Is Required for Dimerization and Substrate Recognition. *Biochem. Biophys. Res. Commun.* **2006**, *343*, 1032–1037.
- (17) Guo, Q.; Manolopoulou, M.; Bian, Y.; Schilling, A. B.; Tang, W.-J. Molecular Basis for the Recognition and Cleavages of IGF-II, TGF-A, and Amylin by Human Insulin-Degrading Enzyme. *J. Mol. Biol.* **2010**, *395*, 430–443.
- (18) Noinaj, N.; Bhasin, S. K.; Song, E. S.; Scoggin, K. E.; Juliano, M. A.; Juliano, L.; Hersh, L. B.; Rodgers, D. W. Identification of the Allosteric Regulatory Site of Insulysin. *PLoS One* **2011**, *6*, e20864.
- (19) Manolopoulou, M.; Guo, Q.; Malito, E.; Schilling, A. B.; Tang, W.-J. Molecular Basis of Catalytic Chamber-Assisted Unfolding and

- Cleavage of Human Insulin by Human Insulin-Degrading Enzyme. *J. Biol. Chem.* **2009**, *284*, 14177–14188.
- (20) Song, E. S.; Juliano, M. A.; Juliano, L.; Fried, M. G.; Wagner, S. L.; Hersh, L. B. ATP Effects on Insulin-Degrading Enzyme Are Mediated Primarily through Its Triphosphate Moiety. *J. Biol. Chem.* **2004**, *279*, 54216–54220.
- (21) Cornista, J.; Ikeuchi, S.; Haruki, M.; Kohara, A.; Takano, K.; Morikawa, M.; Kanaya, S. Cleavage of Various Peptides with Pitrilysin from Escherichia Coli: Kinetic Analyses Using Beta-Endorphin and Its Derivatives. *Biosci. Biotechnol. Biochem.* **2004**, *68*, 2128–2137.
- (22) Shen, Y.; Joachimiak, A.; Rosner, M. R.; Tang, W.-J. Structures of Human Insulin-Degrading Enzyme Reveal a New Substrate Recognition Mechanism. *Nature* **2006**, *443*, 870–874.
- (23) Camberos, M. C.; Perez, A. A.; Udrisar, D. P.; Wanderley, M. I.; Cresto, J. C. ATP Inhibits Insulin-Degrading Enzyme Activity. *Exp. Biol. Med. (Maywood)* **2001**, *226*, 334–341.
- (24) Del Carmen Camberos, M.; Cresto, J. C. Insulin-Degrading Enzyme Hydrolyzes ATP. *Exp. Biol. Med. (Maywood, NJ, U. S.)* **2007**, *232*, 281–292.
- (25) Song, E. S.; Rodgers, D. W.; Hersh, L. B. Mixed Dimers of Insulin-Degrading Enzyme Reveal a Cis Activation Mechanism. *J. Biol. Chem.* **2011**, *286*, 13852–13858.
- (26) Neant-Fery, M.; Garcia-Ordoñez, R. D.; Logan, T. P.; Selkoe, D. J.; Li, L.; Reinstatler, L.; Leissring, M. A. Molecular Basis for the Thiol Sensitivity of Insulin-Degrading Enzyme. *Proc. Natl. Acad. Sci. U. S. A.* **2008**, *105*, 9582–9587.
- (27) Hamel, F. G.; Bennett, R. G.; Duckworth, W. C. Regulation of Multicatalytic Enzyme Activity by Insulin and the Insulin-Degrading Enzyme. *Endocrinology* **1998**, *139*, 4061–4066.
- (28) Noinaj, N.; Song, E. S.; Bhasin, S.; Alper, B. J.; Schmidt, W. K.; Hersh, L. B.; Rodgers, D. W. Anion Activation Site of Insulin-Degrading Enzyme. *J. Biol. Chem.* **2012**, *287*, 48–57.
- (29) Berman, H. M. The Protein Data Bank. *Nucleic Acids Res.* **2000**, *28*, 235–242.
- (30) Dorman, N. SWISS-MODEL and the Swiss-PdbViewer: An Environment for Comparative Protein Modeling. *Biotechniques* **2012**, *53*, 69.
- (31) Case, D. A.; Darden, T. A.; Cheatham, T. E., III; Simmerling, C. L.; Wang, J.; Duke, R. E.; Luo, R.; Walker, R. C.; Zhang, W.; Merz, K. M.; Roberts, B.; Hayik, S.; Roitberg, A.; Seabra, G.; Swails, J.; Goetz, A. W.; Kolossváry, I.; Wong, K. F.; Paesani, F.; Vanicek, J.; Wolf, R. M.; Kollman, P. A. AMBER 12; 2012.
- (32) Morris, G. M.; Huey, R.; Lindstrom, W.; Sanner, M. F.; Belew, R. K.; Goodsell, D. S.; Olson, A. J. AutoDock4 and AutoDockTools4: Automated Docking with Selective Receptor Flexibility. *J. Comput. Chem.* **2009**, *30*, 2785–2791.
- (33) Chen, V. B.; Arendall, W. B.; Headd, J. J.; Keedy, D. A.; Immormino, R. M.; Kapral, G. J.; Murray, L. W.; Richardson, J. S.; Richardson, D. C. MolProbity: All-Atom Structure Validation for Macromolecular Crystallography. *Acta Crystallogr., Sect. D: Biol. Crystallogr.* **2010**, *66*, 12–21.
- (34) Mahoney, M. W.; Jorgensen, W. L. A Five-Site Model for Liquid Water and the Reproduction of the Density Anomaly by Rigid, Nonpolarizable Potential Functions. *J. Chem. Phys.* **2000**, *112*, 8910–8922.
- (35) Adelman, S. A.; Doll, J. D. Generalized Langevin Equation Approach for Atom/solid-Surface Scattering: General Formulation for Classical Scattering off Harmonic Solids. *J. Chem. Phys.* **1976**, *64*, 2375.
- (36) Berendsen, H. J. C.; Postma, J. P. M.; van Gunsteren, W. F.; DiNola, A.; Haak, J. R. Molecular Dynamics with Coupling to an External Bath. *J. Chem. Phys.* **1984**, *81*, 3684.
- (37) Pang, Y. P.; Xu, K.; Yazal, J. E.; Prendergast, F. G. Successful Molecular Dynamics Simulation of the Zinc-Bound Farnesyltransferase Using the Cationic Dummy Atom Approach. *Protein Sci.* **2000**, *9*, 1857–1865.
- (38) Meagher, K. Development of Polyphosphate Parameters for Use with the AMBER Force Field. *J. Comput. Chem.* **2003**, *24*, 1016–1025.
- (39) Dang, L. X. Mechanism and Thermodynamics of Ion Selectivity in Aqueous Solutions of 18-Crown-6 Ether: A Molecular Dynamics Study. *J. Am. Chem. Soc.* **1995**, *117*, 6954–6960.
- (40) Åqvist, J.; Åqvist, J. Ion-Water Interaction Potentials Derived from Free Energy Perturbation Simulations. *J. Phys. Chem.* **1990**, *94*, 8021–8024.
- (41) Frishman, D.; Argos, P. Knowledge-Based Protein Secondary Structure Assignment. *Proteins* **1995**, *23*, 566–579.
- (42) Humphrey, W.; Dalke, A.; Schulten, K. VMD: Visual Molecular Dynamics. *J. Mol. Graphics* **1996**, *14*, 33–38 27–28..
- (43) Patey, G. N.; Valleau, J. P. A Monte Carlo Method for Obtaining the Interionic Potential of Mean Force in Ionic Solution. *J. Chem. Phys.* **1975**, *63*, 2334.
- (44) Torrie, G.; Valleau, J. Nonphysical Sampling Distributions in Monte Carlo Free-Energy Estimation: Umbrella Sampling. *J. Comput. Phys.* **1977**, *23*, 187–199.
- (45) Kumar, S.; Rosenberg, J. M.; Bouzida, D.; Swendsen, R. H.; Kollman, P. A. THE Weighted Histogram Analysis Method for Free-Energy Calculations on Biomolecules. I. The Method. *J. Comput. Chem.* **1992**, *13*, 1011–1021.
- (46) Jeffrey, G. A. *An Introduction to Hydrogen Bonding*; Oxford University Press: 1997; p 303.
- (47) Bora, R. P.; Prabhakar, R. Elucidation of Interactions of Alzheimer Amyloid Beta Peptides (Abeta40 and Abeta42) with Insulin Degrading Enzyme: A Molecular Dynamics Study. *Biochemistry* **2010**, *49*, 3947–3956.
- (48) Song, E.-S.; Juliano, M. A.; Juliano, L.; Hersh, L. B. Substrate Activation of Insulin-Degrading Enzyme (insulysin). A Potential Target for Drug Development. *J. Biol. Chem.* **2003**, *278*, 49789–49794.
- (49) Hashimoto, N.; Robinson, F. W.; Shibata, Y.; Flanagan, J. E.; Kono, T. Diversity in the Effects of Extracellular ATP and Adenosine on the Cellular Processing and Physiologic Actions of Insulin in Rat Adipocytes. *J. Biol. Chem.* **1987**, *262*, 15026–15032.
- (50) Udrisar, D. P.; Wanderley, M. I. Fluoride and Phosphatidylserine Induced Inhibition of Cytosolic Insulin-Degrading Activity. *Acta Physiol., Pharmacol. Ther. Latinoam.* **1992**, *42*, 183–196.
- (51) Yao, H.; Hersh, L. B. Characterization of the Binding of the Fluorescent ATP Analog TNP-ATP to Insulysin. *Arch. Biochem. Biophys.* **2006**, *451*, 175–181.
- (52) Roychaudhuri, R.; Yang, M.; Condon, M. M.; Teplow, D. B. Structural Dynamics of the Amyloid B-Protein Monomer Folding Nucleus. *Biochemistry* **2012**, *51*, 3957–3959.
- (53) Urbanc, B.; Cruz, L.; Teplow, D. B.; Stanley, H. E. Computer Simulations of Alzheimer's Amyloid Beta-Protein Folding and Assembly. *Curr. Alzheimer Res.* **2006**, *3*, 493–504.
- (54) Crescenzi, O.; Tomaselli, S.; Guerrini, R.; Salvadori, S.; D'Ursi, A. M.; Temussi, P. A.; Picone, D. Solution Structure of the Alzheimer Amyloid Beta-Peptide (1–42) in an Apolar Microenvironment. Similarity with a Virus Fusion Domain. *Eur. J. Biochem.* **2002**, *269*, 5642–5648.
- (55) Wei, G.; Shea, J.-E. Effects of Solvent on the Structure of the Alzheimer Amyloid-{beta}(25–35) Peptide. *Biophys. J.* **2006**, *91*, 1638–1647, DOI: 10.1529/biophysj.105.079186.
- (56) Lührs, T.; Ritter, C.; Adrian, M.; Riek-Lohr, D.; Bohrmann, B.; Döbeli, H.; Schubert, D.; Riek, R. 3D Structure of Alzheimer's Amyloid-beta(1–42) Fibrils. *Proc. Natl. Acad. Sci. U. S. A.* **2005**, *102*, 17342–17347.
- (57) Lee, C.; Ham, S. Characterizing Amyloid-Beta Protein Misfolding from Molecular Dynamics Simulations with Explicit Water. *J. Comput. Chem.* **2011**, *32*, 349–355.
- (58) Potocyan, D. A.; Zhuravlev, P. I.; Papoian, G. A. Computing Free Energy of a Large-Scale Allosteric Transition in Adenylate Kinase Using All Atom Explicit Solvent Simulations. *J. Phys. Chem. B* **2012**, *116*, 1709–1715.
- (59) Arora, K.; Brooks, C. L. Large-Scale Allosteric Conformational Transitions of Adenylate Kinase Appear to Involve a Population-Shift Mechanism. *Proc. Natl. Acad. Sci. U. S. A.* **2007**, *104*, 18496–18501.

- (60) Henkelman, G.; Jónsson, H. Improved Tangent Estimate in the Nudged Elastic Band Method for Finding Minimum Energy Paths and Saddle Points. *J. Chem. Phys.* **2000**, *113*, 9978.